

RSC Advances



This is an *Accepted Manuscript*, which has been through the Royal Society of Chemistry peer review process and has been accepted for publication.

Accepted Manuscripts are published online shortly after acceptance, before technical editing, formatting and proof reading. Using this free service, authors can make their results available to the community, in citable form, before we publish the edited article. This *Accepted Manuscript* will be replaced by the edited, formatted and paginated article as soon as this is available.

You can find more information about *Accepted Manuscripts* in the [Information for Authors](#).

Please note that technical editing may introduce minor changes to the text and/or graphics, which may alter content. The journal's standard [Terms & Conditions](#) and the [Ethical guidelines](#) still apply. In no event shall the Royal Society of Chemistry be held responsible for any errors or omissions in this *Accepted Manuscript* or any consequences arising from the use of any information it contains.

ARTICLE

Design of core-shell magnetic mesoporous silica hybrids for pH and UV-light stimuli-responsive cargo release†

Madhappan Santha Moorthy,^a Hak-Bong Kim,^b Jae-Ho Bae,^b Sun-Hee Kim^b and Chang-Sik Ha^{*a}

This paper reports a controlled drug release strategy through the guest diffusion pathways with a “three-in-one” system by combining three advantages together in a single entity. The designed system was composed of superparamagnetic Fe₃O₄ nanoparticles as the core, mesoporous silica hybrid as the shell with specific functional moieties, and external trigger (UV-light) responsive functional derivatives as the nanoregulators. The magnetic mesoporous silica hybrid nanospheres (MSH@Azo-CA) were quite responsive to external stimuli such as (i) UV-light and (ii) pH triggered drug release. The core-shell mesoporous silica hybrid nanospheres were used as a drug carrier for the loading and controlled release of model cargo (e.g. doxorubicin hydrochloride (DOX)/Rh123) because of its combined external (UV-light) and internal (cellular pH) stimuli-responsive behavior and biocompatibility. The experimental study showed that the drug release behavior depends mainly on the UV-light (365 nm)-actuated ‘*trans*’ conformation and ‘*cis*’ conformation of the nanoregulators (chrysoidine derivatives) and the intracellular pH of the release medium. The presence of external and internal triggers can result in the good controlled release of loaded cargoes to the target sites. The cytotoxicity of the synthesized core-shell hybrid mesoporous silica nanospheres were examined using MCF-7 cells. The intracellular uptake and release process was observed by confocal laser scanning microscopy (CLSM). In addition, the presence of a magnetic core means that these silica hybrid nanospheres have potential use in the efficient targeted delivery of anticancer agents that can be directed by an external magnetic field for the delivery with a dose predetermined by the ‘ON’ and ‘OFF’ command driven by the external UV-light trigger.

Introduction

Recent studies have focused mainly on the intracellular delivery of membrane-impermeable therapeutic agents, proteins, genes, and other biomolecules for a range of potential clinical applications.¹ These reports have revealed successful intracellular delivery using a carrier system that can deliver both efficiently and selectively the loaded therapeutic agents and biomolecules to the specific target sites.^{2,3} Such a carrier system can reduce tissue damage considerably, avoid premature leakage of the loaded drugs before reaching the target site, and eliminate side effects to the non-target tissues.⁴ Many reports on the preparation of various drug carrier systems exist, such as dendrimers,⁵ liposomes,⁶ polymeric nanoparticles,⁷ core-shell nanoparticles,⁸ magnetic nanocomposites and mesoporous silicas.^{9,10} Generally, an efficient drug delivery system should possess a large drug loading capacity with high efficiency, and release it at a specific target site in a controlled manner.¹¹ A recent breakthrough in this field is the successful utilization of inorganic nanomaterials, such as mesoporous silica

nanoparticle (MSN)-based drug delivery vehicles,^{12,13} owing to its unique properties of MSNs, such as large surface area, tunable pore sizes and versatile surface modification chemistry and excellent biocompatibility make them desirable for a range of applications.¹⁴

The current strategy is to prepare core-shell structured magnetic mesoporous silica nanoparticles (Fe₃O₄@MSNs) for specific applications that have attracted intense research interest because of the combined properties of superparamagnetic core and mesoporous silica shell structures.^{15,16} The magnetic core provides contrast enhancement for magnetic resonance imaging (MRI) applications as well as potential magnetic targeting through the application of an external magnetic field.¹⁷ The outer mesoporous silica shell can be utilized effectively for the incorporation of functional groups and a large drug loading owing to its high surface area and large pore volume, thermal and photo stability, and excellent biocompatibility. Therefore, core-shell Fe₃O₄@MSN can be considered as highly promising nanocarrier system for drug delivery.¹⁸⁻²⁰ The delivery of some

toxic anticancer drugs requires “zero release” until reaching the target sites to avoid undesirable side effects on normal cells. Therefore, it is essential to incorporate some specific functional groups into the inner/outer mesopores, which could act as the regulators to protect the loaded drugs into the mesochannels and avoid premature leakage. For this purpose, a range of polymer materials and some organic functionalities are incorporated onto the exterior surface of the silica shells.²¹ Very recently, Zhuo *et al.* reported cyclodextrin-covered mesoporous silica nanoparticles²² modified with photocleavable and external voltage responsive functional units for dual-stimulated release system for controlled cargo release. The same group also reported glucose- and pH responsive delivery system based on cross-linked polymeric network capped MSN for controlled release of guest molecules.²³ Even though these types of modifications have some drawbacks, such as more complicated synthesis steps and uncontrollable drug release, once the cap has been removed.²⁴

A range of internal/external stimuli, such as pH, light, enzyme and redox activation, have been used successfully for the controlled release of drugs from a carrier system.²⁵ Among them, pH and light are considered efficient stimuli for therapeutic applications.^{26,27} Several pH/light responsive drug delivery systems using various pH-sensitive or light-responsive organic molecules have been reported.²⁸ Diazobenzene derivatives, which have a $-N=N-$ bond with a phenyl ring on either side, are well-known light sensitive molecules. When irradiating with UV-light, they undergo ‘*trans-to-cis*’ photoisomerization in aqueous environments. Based on this phenomenon, when such diazobenzene derivatives are incorporated into the nanocarrier systems that can undergo ‘*trans-to-cis*’ photoisomerization, the release of the loaded drugs would be expected to take place in a controlled manner after exposure to an external UV-light switch. The carboxylic acid (CA) groups and amine (NH_2) groups are considered important functional groups in organic chemistry because they can interact with guest molecules through hydrogen bonding or electrostatic interactions. The incorporation of specific functional groups into drug carrier systems can enhance the drug loading and prevent the drug molecules from premature release compared to non-functionalized silica carriers. The incorporation of specific functional groups into drug carrier systems can enhance the drug loading and prevent the drug molecules from premature release compared to non-functionalized silica carriers.

This paper reports core-shell magnetic mesoporous silica hybrid (MSH) nanospheres integrated with 3-(triethoxysilyl)propylsuccinic anhydride (SATES) functionalities, which would be more useful for deriving carboxylic acid groups and amide groups ($-CONH$) together onto the mesochannel surfaces by the covalent incorporation of amine group-containing functionalities. For this purpose, amine groups containing UV-light sensitive diazo derivatives (Azo) together with covalently incorporated succinic anhydride parts of the organosilane functionalities were used to introduce surface carboxylic acid groups and amide groups to the mesopore surfaces. Derivatized CA groups, $-CONH-$ groups,

and incorporated chrysoidine derivatives (Ph-N=N-Ph) with $-NH_2$ groups were combined to play two important roles in controlled and sustained drug release from the prepared hybrid mesoporous silica nanospheres. First, the derivatized surface CA, $-CONH-$ and the existing $-NH_2$ groups act together as drug binding sites through H-bonding/electrostatic interactions to prevent the premature leakage of the encapsulated drugs from the mesochannels. Second, the incorporated diazo derivatives act as a UV-light sensitive organic functionalities to protect the loaded drugs in the mesochannels and release them to the specific target sites in a controlled manner over a long period of time by external UV-light stimuli. The pH-induced and UV-light-controlled release properties of the prepared hybrid MSH@Azo-CA nanospheres were examined using Rh123/DOX as the model cargo. MCF-7 cells were selected to gain knowledge on the cellular internalization and cytotoxicity of the synthesized hybrid MSH@Azo-CA nanospheres.

Experimental

Materials and Methods

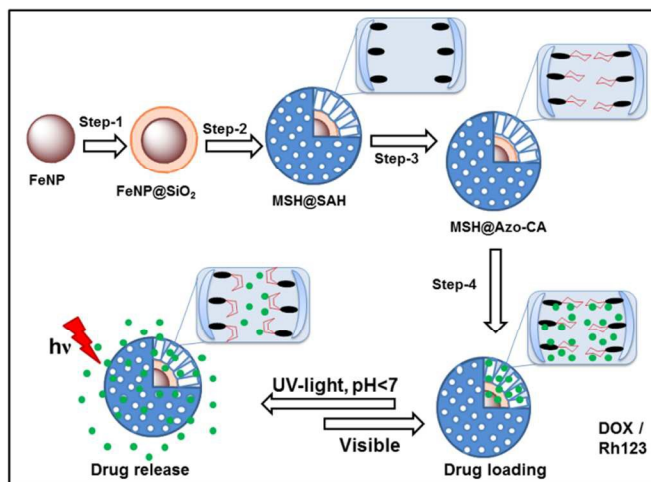
3-(triethoxysilyl)propylsuccinic anhydride (SATES), tetraethyl orthosilicate (TEOS), cetyltrimethylammonium bromide (CTAB), $FeCl_3 \cdot 6H_2O$, ethylene glycol, ammonium hydroxide (NH_4OH , 25 wt%), ammonium nitrate (NH_4NO_3), sodium acetate (NaOAc), absolute ethanol, chrysoidine, rhodamine 123 (Rh123) and doxorubicin hydrochloride (DOX) were purchased from Aldrich Chemicals, USA. All chemicals were used as received.

Synthesis of Fe_3O_4 nanoparticles

The magnetic Fe_3O_4 nanoparticles were prepared by a solvothermal reaction.²⁹ Typically, 0.65 g (4.0 mmol) of $FeCl_3 \cdot 6H_2O$ salt was dissolved in 20 ml of ethylene glycol under magnetic stirring until the solution became clear. To this, 1.80 g of sodium acetate was added with constant magnetic stirring followed by stirring for a further 1 h to form a homogeneous solution. Approximately 0.25 g trisodium citrate was added. The resulting mixture was stirred at room temperature for 5 h to form a homogeneous dispersion. The homogeneous yellow solution obtained was transferred to a Teflon-lined stainless-steel autoclave (50 ml capacity) and heated at 200 °C for 8 h. The obtained black particles were washed five times with ethanol and deionized water, and then dried overnight in a vacuum at 60 °C.

Synthesis of core-shell magnetic mesoporous organosilica hybrid nanoparticles (MSH@SAH)

The $Fe_3O_4@SiO_2$ magnetic mesoporous silica nanoparticles were prepared using a slight modification of the procedure reported elsewhere.³⁰ First, 0.2 g of Fe_3O_4 nanoparticles were dispersed in a mixture of ethanol (80 mL), deionized water (20 mL) and ammonia solution (2.4 mL, 28%) by ultrasonication for 1 h. To this solution, 0.8 mL of TEOS was added dropwise. After stirring for 6 h, the products were collected and washed with ethanol and deionized water, and then dried overnight at 60 °C. Second, 0.2 g of the as-synthesized $Fe_3O_4@SiO_2$ particles were dispersed in 120 mL ethanol by ultrasonication. Subsequently, 2.4 mL of a concentrated ammonia solution (28%) was added to form solution A. Next, 0.6 g CTAB was dispersed in 160 mL of deionized water with constant magnetic



Scheme 1. Schematic diagram of the synthesis of core-shell MSH@Azo-CA nanosphere and drug/dye loading and release behavior under combined pH and UV-light trigger. FeNP denotes the Fe_3O_4 nanoparticles.

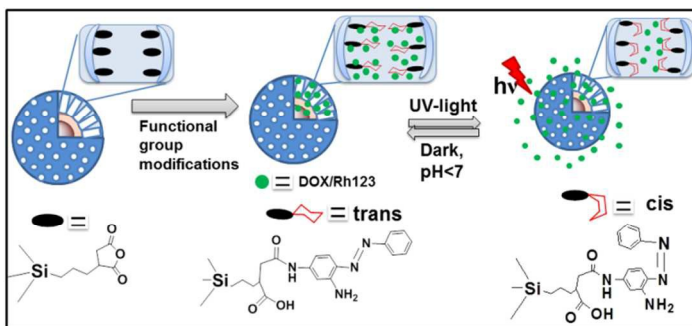
stirring to form solution B. Solution B was added to solution A with vigorous stirring for 6 h. To this solution, the premixed solution of SATES and TEOS to afford a 30 mol% of SATES/(TEOS + SATES) was added drop wise to the dispersion with vigorous stirring. The molar composition of the reaction mixture was 1 (SATES + TEOS) : 0.125 CTAB : 69 NH_3 : 525 H_2O . The resulted mixture was stirred for 6 h at 35 °C and for another 6 h at 80 °C. The products were collected with a magnet bar and washed with ethanol and deionized water to remove the non-magnetic byproducts followed by drying at 60 °C. Third, an alcoholic solution of ammonium nitrate was used to exchange the surfactant molecules from the as-synthesized nanoparticles. For this process, 1.0 g of the as-synthesized nanoparticles was dispersed in 150 ml of ethanol (95%) containing 0.3 g NH_4NO_3 , and the mixture was stirred for 1 h at 60 °C. The product was separated by an external magnet and washed with cold ethanol. The above process was repeated three times. The obtained product was called MSH@SAH (Scheme 1, Step-1 and Step-2).

Synthesis of the dual stimuli responsive functional groups incorporated magnetic mesoporous organosilica hybrid nanospheres (MSH@Azo-CA)

1.0 g of the MSH@SAH nanospheres was allowed to react with the chrysoidine derivative (0.3 g, 1.2 mmol) in 40 ml tetrahydrofuran (THF) at room temperature for 6 h. During this modification reaction, the active carboxylic acid groups and amide groups were produced on the mesochannel surfaces by a reaction of the primary amine groups of chrysoidine derivatives with the succinic anhydride parts of the SATES functionalities that were integrated into the mesoporous silica shell (Scheme 1, Step-2 and Scheme 2). The chrysoidine derivative-modified product was collected by an external magnet and washed thoroughly with THF and ethanol to remove the unreacted molecules, followed by drying overnight under vacuum. The modified product was labelled as MSH@Azo-CA.

Dye/Drug loading into the MSH@Azo-CA

Rhodamine 123 (Rh123) was selected as the model cargo to evaluate the drug loading and release behaviour³¹⁻³³ from the carboxylic acid



Scheme 2. Schematic diagram of the MSH@Azo-CA nanospheres modified with chrysoidine functional derivatives and their drug/dye molecules binding/release behavior from the drug interacting functional sites.

groups containing MSH@Azo-CA samples. Rh123 was encapsulated into the synthesized magnetic mesoporous silica hybrid nanospheres by soaking 100 mg of the MSH@Azo-CA particles in 10 ml (2 mg mL^{-1}) of a Rh123 dye solution in ethanol at room temperature for 24 h. The dye loading process was carried out in the presence of UV light, such that the diazo part of the chrysoidine derivatives was in a state of dynamic movement (Scheme1, Step-4). After loading, the Rh123 encapsulated particles were separated by magnetic decantation and washed with ethanol until the supernatant appeared colorless. Similarly, DOX-encapsulated MSH@Azo-CA nanospheres were prepared using the same process, except that they were dispersed in deionized water instead. After the loading process, the amount of encapsulated dye/drug was determined by subtracting the mass of the Rh123/DOX in the supernatant from the total mass of the Rh123/DOX in the initial solution. The amount of Rh123 loaded was analyzed by UV-vis spectroscopy at the wavelength of 506 nm. Similarly, the DOX loading was evaluated at a wavelength of 482 nm. The calculated amount of loaded Rh123 and DOX into the MSH@Azo-CA was 125 mg/g and 132 mg/g, respectively (Table 1).

In vitro release experiment

25 ml of phosphate buffered saline (PBS) with different pHs (pH 7.4, 6 and 5) was used to measure the Rh123 release profile. The *in vitro* release experiment was performed by placing Rh123-loaded MSH@Azo-CA samples in two vials in PBS buffer at pH 7.4, 6 and 5, respectively, and placed near a magnet in the corner of the vials. One vial was exposed to UV-light (365 nm) to activate the existing chrysoidine derivatives present in the mesoporous channels of the MSH@Azo-CA, whereas the other vial was placed in the dark and used as a control sample. The release rate was monitored for 24 h at predetermined time intervals. Two sets of the cargo release experiments were conducted to evaluate the combined effects of both the medium pH and UV-light stimuli, i.e. (i) the effect of pH to hold and release the existing functional carboxylic acid groups, amine and imine groups that act as binding sites for dyes/drugs, and (ii) the effect of the external UV-light stimuli on the light sensitive chrysoidine derivatives that could be used to protect/release the loaded dyes/drugs in a controlled manner (Scheme 2).

Cell culture

MCF-7 cell line was used as a model cellular system to evaluate the *in vitro* cytotoxicity of the MSH@Azo-CA nanospheres by an 3-(4,5-dimethylthiazole-2-yl)-2,5-diphenyl tetrazolium bromide (MTT) assay. The MCF-7 cells were cultured in cell culture flasks at 37 °C in a humidified atmosphere containing 5% CO₂/95% air with a minimum essential medium (MEM) containing 10% fetal bovine serum, 100 U mL⁻¹ penicillin G and 100 µg mL⁻¹ streptomycin.

Cytotoxicity assay

The anticancer drug DOX-loaded MSH@Azo-CA samples were used to examine the *in vitro* cytotoxicity. All the experiments were carried out with the following sample designation: MSH@Azo-CA – the cells treated with the blank carrier particles; and MSH@Azo-CA-DOX – the cells treated with DOX loaded nanosphere samples. All the samples were incubated either in the dark at all times or were incubated in the dark except when subjected to UV-light irradiation for 30 min, i.e. the culture plates were placed below the Spectroline UV lamp model ENF-240e (115 V, 60 Hz, 0.2 A, measured light intensity = 1.0 mW cm⁻¹). At the same time, the ‘dark’ samples were kept in the dark, outside the incubator. The sample-treated cells were then protected from light and kept back for additional incubation for 20 h at 37 °C.

The cell cytotoxicity was evaluated by MTT assay. For this study, MCF-7 cells were plated into 24-well plates at a density of 1 × 10⁴ cells per well in 1.0 mL culture medium and incubated for 24 h. 1.0 mL of MEM medium containing blank and DOX loaded MSH@Azo-CA samples at a concentration of 1, 10, 50 and 100 µg mL⁻¹ was then added to each well. The blank samples, i.e. the samples treated without the drug, and the DOX-loaded samples were treated in the same manner during all steps of the cell culture experiments. Subsequently, the medium was removed, 200 µL dimethyl sulfoxide (DMSO) was added to each well, and the absorbance was then measured using a microplate reader (Dynatech ELISA reader, model MR7000) at a wavelength of 570 nm. Three replicates were counted for each sample. The cell viability was calculated using the following equation:

$$\text{Cell viability (\%)} = \text{OD}_{\text{treated}} / \text{OD}_{\text{control}} \times 100$$

where OD_{treated} was obtained for all the cells treated by the DOX-loaded MSH@Azo-CA for 24 h. The OD_{control} was obtained for the cells treated with the sample without the DOX loading, and the other culture conditions were the same. (OD = optical density).

Cellular uptake experiment

To track the *in vitro* cellular uptake process, the MCF-7 cells were plated in a cell culture dish using Dulbecco's modified Eagle's medium containing 10% fetal bovine serum supplemented with 100 U mL⁻¹ penicillin G and 100 µg mL⁻¹ streptomycin in 6-well plates, and incubated at 37 °C in an atmosphere containing 5% CO₂/95% air. The medium was then replaced with 0.5 ml of culture serum-free medium containing 100 µg mL⁻¹ of the Rh123-encapsulated MSH@Azo-CA-Rh123

particles. In addition, the cells were subjected to UV-light irradiation for 30 min. After incubation for a further 3 h, the culture medium was removed and the cells in the cell culture dishes were washed twice with a PBS solution (pH 7.0, 0.1 M). The cells were then visualized and fluorescence images of the cells were obtained by confocal laser scanning microscopy (Leica, TCS-SP2).

Characterization

Fourier transform infrared (FTIR JASCO FTIR 4100) spectroscopy was performed using KBr pellets. The X-ray diffraction (XRD, Bruker AXN) patterns were obtained using CuKα irradiation. Surface analysis of the nanospheres was performed by nitrogen isothermal adsorption on a Nova 4000e surface area and pore analyzer. The surface areas were calculated using the Brunauer-Emmet-Teller (BET) approach and the pore size distributions were obtained from an analysis of the adsorption branch using the Barrett-Joyner-Halenda (BJH) method. The morphology of the materials was observed by scanning electron microscopy (SEM, JEOL 6400). The synthesized samples were visualized by transmission electron microscopy (TEM, JEOL 2010). Thermogravimetric analysis (TGA, Perkin-Elmer Pyris Diamond) was carried out from 100–800 °C (10 °C min⁻¹) in flowing air. The particle size distribution in the suspension was measured by dynamic light scattering (DLS) on a Malvern Zetasizer Nano-ZS (Malvern Instruments). The magnetic measurements were performed with a super conducting quantum interference device (SQUID) magnetometer (Quantum design, MPMS XL). The UV-vis spectral measurements were performed using a HITACHI 3220UV spectrometer.

Results and discussion

FTIR spectroscopy was performed to confirm the formation of the mesoporous silica hybrid shell onto the Fe₃O₄ nanoparticles as the core and integrated

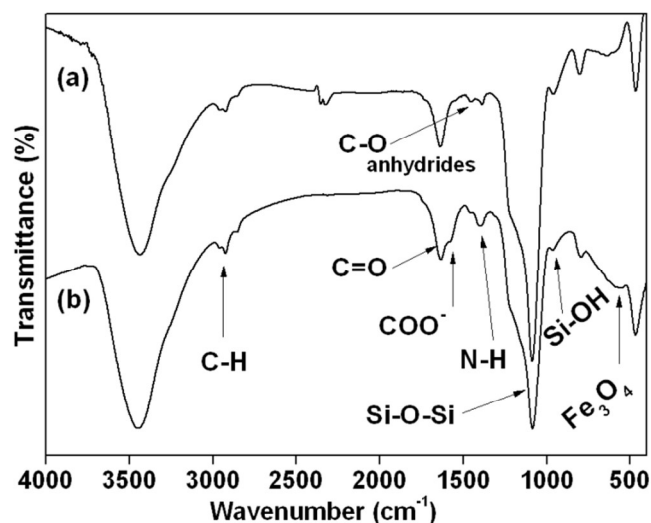


Figure 1. FTIR spectra of the (a) MSH@SAH and (b) MSH@Azo-CA nanospheres.

organosilane functional groups in the silica shell. As shown in Figure 1, the characteristic peak at 1083 cm^{-1} was assigned to the vibration bands of Si-O-Si, whereas the peak at 957 cm^{-1} belongs to Si-OH stretching vibration mode, suggesting the formation of a silica shell on the magnetic nanoparticles (Figure 1(a)). The stretching vibration peaks in the range, $1230\text{--}1370\text{ cm}^{-1}$, corresponding to the succinic anhydride groups,³⁴ further confirmed that succinic anhydride groups containing organosilane functionalities (SATES) had been integrated into the MSH@SAH particles (Figure 1(a)). Furthermore, after modifying the chrysoidine derivatives, the succinic anhydride peak at 1230 cm^{-1} almost disappeared in the FTIR spectrum of MSH@Azo-CA, while new stretching vibration bands at 1644 cm^{-1} and 1395 cm^{-1} for C=O and N-H, respectively, were observed (Figure 1(b)). Moreover, a new broad peak appeared at 1580 cm^{-1} , which overlapped almost completely with the water peak, indicating the formation of carboxylate ($-\text{COO}^-$) groups onto the mesochannel surfaces by a reaction of succinic anhydride with the amine parts of chrysoidine derivatives (Figure 1(b)).³⁵ The stretching vibration band at 558 cm^{-1} was assigned to the presence of Fe_3O_4 nanoparticles in the core of the MSH@Azo-CA nanospheres.³⁶ For comparison, the FTIR spectrum of the control Fe_3O_4 @MSN was prepared without organic functional groups (Figure S1, ESI†). The vibration peaks at 1085 cm^{-1} and 955 cm^{-1} indicate the formation of Si-O-Si and Si-OH groups in the silica shell on the Fe_3O_4 nanoparticles without any organic functional groups.

Figure 2 shows the low angle X-ray diffraction (XRD) patterns of the hybrid MSH@SAH (Figure 2A(a)) and MSH@Azo-CA (Figure 2A(b)) nanospheres. The clear intense diffraction peak (100) at $1.19^\circ 2\theta$ with a d-spacing of 38.5 \AA suggests the formation of hexagonal mesostructural arrangements in the silica shell. After modification of the chrysoidine derivatives to produce a nanocontroller in the mesochannels, the peak intensity and d-spacing decreased slightly to $1.21^\circ 2\theta$ and 36.4 \AA , respectively (Figure 2A(b)). This suggests that the modification reaction occurred with the existing anhydride groups of the SATES moieties of MSH@SAH. These results show that the mesostructural arrangement of the hybrid MSH@Azo-CA nanospheres had been maintained after the functional derivative modification process. The presence of a magnetic core in the core-shell structure of the silica hybrid nanospheres was confirmed further by the higher angle XRD patterns from 10° to $70^\circ 2\theta$ on pure Fe_3O_4 nanoparticles and MSH@Azo-CA nanospheres (Figure 2(B)). The wide angle XRD patterns showed that the prepared nanospheres had similar diffraction peaks to those of the pure Fe_3O_4 nanoparticles.³⁷ The XRD peaks at 30.3° , 35.7° , 43.5° , 54.2° , 57.4° and $63.0^\circ 2\theta$ were assigned to the [220], [311], [400], [422], [511] and [440] planes, respectively, which agrees with the JCPDS Card No.19-0629, showing that the Fe_3O_4 nanoparticles have a hexagonal phase structure.³⁸ Figure 3(A) and (B) show the N_2 adsorption-desorption isotherm curves of the MSH@SAH and MSH@Azo-CA nanospheres. Both MSH@SAH and MSH@Azo-CA showed type IV isotherms and H1 hysteresis loops according to IUPAC classifications, indicating the formation of uniform mesopores.

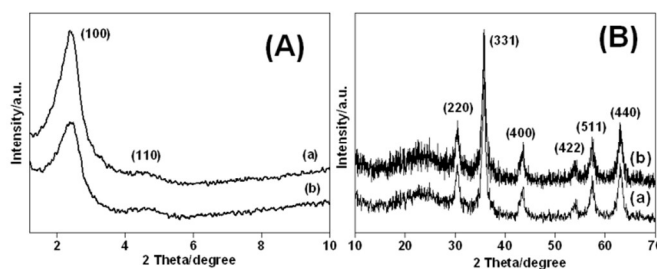


Figure 2. (A) Low-angle X-ray diffraction patterns of the (a) MSH@SAH and (b) MSH@Azo-CA nanospheres. (B) higher angle X-ray diffraction patterns of the (a) pure Fe_3O_4 nanoparticles and (b) MSH@Azo-CA nanospheres.

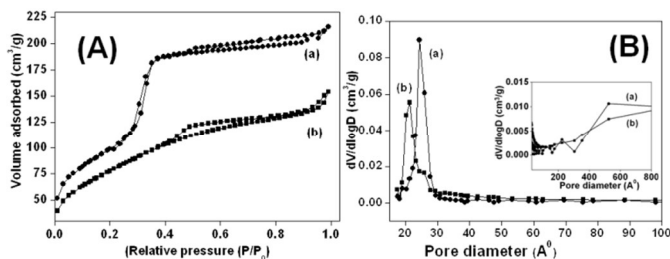


Figure 3. N_2 adsorption-desorption isotherms (A) and pore size distribution (B) curves of the (a) MSH@SAH and (b) MSH@Azo-CA nanospheres.

After modifying the chrysoidine derivative, the isotherm for MSH@Azo-CA showed a decrease in surface area, pore volume and pore diameter. In addition, after modification of the chrysoidine functional derivative, MSH@Azo-CA showed lower nitrogen adsorption and a smaller hysteresis loop, suggesting that the mesopores are partially blocked by modified organic functional derivatives. Table 1 lists the changes in mesopore properties of the MSH@SAH and MSH@Azo-CA. The BET surface area and pore size of the MSH@SAH sample were $586\text{ m}^2\text{ g}^{-1}$ and 2.7 nm , respectively. The surface area and pore size of the MSH@Azo-CA sample were $360\text{ m}^2\text{ g}^{-1}$ and 2.3 nm , respectively (Table 1). This suggests that the chrysoidine functional derivatives on the mesopore channels of the core-shell hybrid MSH@Azo-CA nanospheres had been modified successfully. The existence of a magnetic core in the mesoporous silica shell revealed a second adsorption process, which is characteristic of the textural interparticle meso/macroporosity.³⁹ The bimodal porosity of the core-shell magnetic mesoporous silica nanospheres with small mesopores and large interparticle mesopores/macropores was observed in both isotherms and pore size distributions (Figure 3(A), (B)).

Figure S2(a) (ESI†) shows the surface morphology of the MSH@Azo-CA nanospheres revealing the formation of uniform spherical particles with sizes of $\sim 200\text{--}300\text{ nm}$. Such spherical mesostructural small size nanoparticles obtained are promising for a range of applications. Figure S2(b,c) (ESI†) show typical TEM images of MSH@Azo-CA nanospheres. The TEM image shows the formation of the mesochannel arrangements as well as the existence of Fe_3O_4 nanoparticles as

Table 1. Physicochemical properties of the synthesized core-shell magnetic mesoporous silica material.

| Sample | S_{BET} (m ² /g) | Pore size (nm) | Pore volume (cm ³ /g) | Drug/Dye loading (mg/g) | |
|------------|--------------------------------------|----------------|----------------------------------|-------------------------|-------|
| | | | | DOX | Rh123 |
| MSH@SAH | 586 | 2.7 | 0.38 | --- | --- |
| MSH@Azo-CA | 360 | 2.3 | 0.34 | 132 | 125 |

a core of the synthesized core-shell mesoporous silica hybrids with an outer light contrast silica shell and dark contrast inner core of the Fe₃O₄ nanoparticles. The shell thickness of the outer silica shell is approximately 35-40 nm. SEM and TEM images evidence the successful synthesis of the core-shell mesoporous silica hybrids. The dynamic light scattering study shows the mean particle size of the synthesized core-shell MSH@Azo-CA nanospheres was in the range about ~150-400 nm (Figure S2(d)(ESI†)).

Figure S3(a) and (b) (ESI†) present the thermogravimetric analysis (TGA) curves of MSH@SAH and MSH@Azo-CA. A four-stage weight loss was observed in the TGA profiles. The initial weight loss of approximately 5 wt% at ~100 °C was assigned to the evaporation of physisorbed water or ethanol. The main weight loss observed at temperatures ranging from 120-600 °C was approximately 18.5 wt%, which corresponds to the combined decomposition of the functionalized organic derivatives. The further weight loss at higher temperatures was attributed to carbon residue oxidation and further condensation of silanol network present in the silica-shells. Figure S4A (a),(b) and (c) show the magnetization curves measured at room temperature for Fe₃O₄ nanoparticles, MSH@SAH and MSH@Azo-CA nanospheres. The magnetic behavior of the synthesized samples was characterized using a magnetometer at 300 K. The saturation magnetization of pure Fe₃O₄ nanoparticles, MSH@SAH and MSH@Azo-CA nanospheres were 72.56 emu g⁻¹, 37.62 emu g⁻¹ and 33.51 emu g⁻¹, respectively. None of the samples showed hysteresis in their room temperature magnetization curves, meaning that the hybrid materials exhibit strong superparamagnetism.⁴⁰ The fast separation efficiency of the MSH@Azo-CA nanospheres was tested after dispersing them in water in a cuvette and placed near a magnet. A rapid response (within 30 s) was observed when the magnet bar was placed near the cuvette (Figure S4(B)). This highlights the superparamagnetic behavior of the MSH@Azo-CA nanospheres under an external magnetic field.

Photoisomerization is a process that involves conformational changes for a normal double bond (-N=N-) containing azo based aromatic molecules that undergo 'cis-trans' isomerization upon irradiation with light.⁴¹ The synthesized magnetic mesoporous silica hybrid MSH@Azo-CA nanospheres are composed of photo switchable chrysoidine derivatives as a nanocontroller, and the derived surface carboxylic acid, amine and amide groups play key roles as drug binding sites (Scheme 1). Amine groups containing drug/dye molecules (e.g. DOX or Rh123) were chosen as model cargos to evaluate the importance of the carboxylic acid groups. The

amine and amide groups located in the mesopore channels act as drug binding sites, and the functionalized chrysoidine derivatives are used to protect the payloads in the mesochannels in the MSH@Azo-CA from pre-leakage and allow dual stimuli-responsive release behavior. As shown in Scheme 2, the encapsulated cargo molecules can interact with -COOH, -NH₂ and -NH- groups via H-bonding/electrostatic interactions followed by mesochannel blocking by a 'trans conformation' of photoactive chrysoidine derivatives that prevent premature leakage of the payloads from the mesopore channels of the MSH@Azo-CA carriers. When irradiated with UV-light (365 nm), the 'trans confirmation' of the chrysoidine derivatives undergo 'cis confirmations'. Therefore, the diffusion pathways become open and can release the entrapped cargo molecules from the mesopores. The pH of the release medium will further regulate the release rate by breaking the existing H-bonding/electrostatic interactions between the drugs/dyes and -COOH, -NH₂ and -NH- parts of the functional derivatives.

Two sets of *in vitro* release experiments were performed under two different conditions [(1) (A) dark, pH 7.4, and UV-light, pH 7.4, and (2) (B) dark, pH 6 and 5, and UV-light, pH 6 and 5] to examine the combined stimuli effects on (i) pore blocking/opening efficiency of the functional derivatives (chrysoidine), and (ii) the effect of pHs on the holding/release of the entrapped cargoes from the guest binding sites of the -COOH, -NH₂ and -NH- parts of the organic functional derivatives that exist in the mesopore channels. In Set-1, the combined UV-light trigger and pH-stimuli responsive *in vitro* drug release of the Rh123 loaded MSH@Azo-CA was performed in a PBS solution (i) under dark conditions at pH 7.4 and (ii) in the presence of UV-light (365 nm) at pH 7.4, respectively, for 24 h. Only 12.5 % and 22 % of the loaded Rh123 was released throughout the study time (Figure 4(A)). Strong H-bonding/electrostatic interactions exist between the

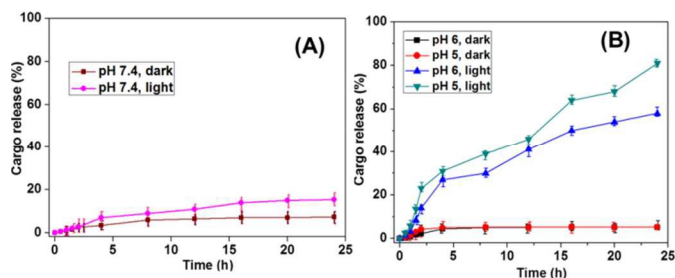


Figure 4. Combined pH and UV-light (365 nm) triggered release profiles of Rh123 from the Rh123-loaded MSH@Azo-CA nanospheres (A) in the dark, pH 7.4 and with UV-light, pH 7.4. (B) in the dark, pH 6 and 5 and with UV-light, pH 6 and 5, respectively.

amine groups of Rh123 and $-\text{COOH}$, $-\text{NH}_2$ and $-\text{NH}-$ of the guest binding sites at pH 7.4. In addition, under dark conditions, the 'diazo' parts of the functionalized chrysoidine derivatives exhibit 'trans-confirmations' and the guest diffusion pathways are blocked almost completely. Moreover, there was no further way to diffuse out the physisorbed cargo molecules from the mesopore channels. The low release (only 12.5 %, 22 %) of Rh123 at pH 7.4 might be due to the release of physisorbed dye molecules into the mesochannel surfaces. The physisorbed molecules can diffuse easily from the mesopore channels under UV-light conditions because the chrysoidine derivatives undergo "cis-confirmation" in the presence of UV-light. Therefore, the diffusion pathways become open and can allow the diffusion of weakly entrapped cargo molecules from the mesochannels. Only 22 % of the Rh123 molecules were released out at the end of the 24 h release period. The majority of the Rh123 molecules were strongly interacted with the existing $-\text{COOH}$, $-\text{NH}_2$ and $-\text{NH}-$ functional groups via H-bonding/electrostatic interactions. Therefore, the loaded dye molecules could not diffuse out freely from the mesochannels at pH 7.4, even in the presence of UV-light. This highlights the crucial role of surface derivatized carboxylic acid groups, as well as amine and imine groups that can keep the guest molecules constrained all times at pH 7.4. The release study clearly showed that the prepared MSH@Azo-CA nanospheres are desirable for drug storage.

In Set-2, a similar set of release experiments was carried out under acidic pH conditions, typically, (i) under dark, pH 6 and 5 and (ii) under UV-light, pH 5.0, respectively. Figure 4(B) shows that ~15.5 % and 16 % of Rh123 was released from the Rh123-loaded MSH@Azo-CA nanocarrier under dark conditions at pH 6 and 5, respectively. The low release of Rh123 was observed due to the 'trans' confirmation of chrysoidine derivatives that almost completely blocked the diffusion pathways. In contrast, an enhanced release (~62% and 84%) of Rh123 was observed at pH 6 and 5, respectively in the presence of UV-light. This reveals that the light sensitive diazo part of the chrysoidine derivatives undergo 'cis-confirmation' in the presence of UV-light (365 nm). Therefore, the guest diffusion pathways turn to open, as illustrated in Scheme 1 and 2. Therefore, Rh123 cargoes can be readily diffuse out from the mesopore channels of the Rh123-loaded MSH@Azo-CA carrier under acidic conditions due to the strong electrostatic repulsive force that exists between the protonated Rh123 and $-\text{NH}_2$ and $-\text{NH}-$ parts of the guest binding sites. Rh123 release was increased significantly from 15.5 % and 16 % to 62 % and 84 % in the presence of the combined UV-light and acidic pH stimuli for 24 h release period at pH 7.4 and pH 6 and 5, respectively, in the presence of UV-light (365 nm). These values were significantly higher than those values observed under dark and light conditions (12.5 % and 16 % for pH 7.4) (Figure 4 (A)). This confirmed the effect of UV-light controlled release of cargoes from these MSH@Azo-CA silica nanocarriers. The 'trans-conformation' of the chrysoidine derivatives under UV-light exposure, the increased spacing of the pore channels of the mesoporous silica to facilitate an enhanced release, and the release triggered by acidic pH stimuli together result in the enhanced release of

Rh123 from the MSH@Azo-CA particles under acidic pH conditions. This suggests that the UV-light triggered release is also pH-based. Such a pH-based drug release is important for cancer treatment, because of the decreased pH environment of the tumor tissue as compared to the normal tissue (pH 7.4). This is the key advantage of the designed MSH@Azo-CA drug carrier, which is more desirable for the storage and safe delivery of toxic anticancer agents for cancer therapy.

In this work, we used Rh123 dye as a model cargo for loading and release experiment because we specifically considered the effect of the drug interacting organic functional sites on the silica surfaces. In our designed silica carrier having $-\text{COOH}$, $-\text{NH}_2$ and $-\text{NH}-$ functional sites, Rh123 dye is relatively specific for interacting the loaded drugs and sensitive to pH-stimuli responsive release. Therefore, we have chosen Rh123 as the model cargo to verify MSH@Azo-CA carriers that would be more useful for loading/release of not only DOX but also any other kind of amine and carboxyl groups containing anticancer drugs.

In vitro cytotoxicity (MTT assay)

The *in-vitro* cytotoxicity of the MSH@Azo-CA was evaluated by a MTT assays on human breast cancer cells (MCF-7 cell lines) using blank and DOX-loaded MSH@Azo-CA samples, respectively, (Figure 5(A and B)). As shown in Figure 5(A), the blank MSH@Azo-CA nanocarriers were almost non-toxic to MCF-7 cells at concentrations of 1-100 $\mu\text{g mL}^{-1}$ after 24 h incubation. In the presence of UV-light under pH 6.0 conditions, about ~2 % and ~8 % cytotoxicity was observed (Figure 5(A)). This might be caused by UV-light or by MSH@Azo-CA nanospheres under acidic conditions. These results suggest that the MSH@Azo-CA carriers are non-toxic. On the other hand, the DOX-loaded MSH@Azo-CA samples showed a significantly enhanced cytotoxicity of approximately 10 %, 45 %, 62 % and 86 % at DOX-loaded nanocarrier concentrations of 1, 10, 50 and 100 $\mu\text{g mL}^{-1}$, respectively, under combined stimuli, such as decreased pH (pH 6.0) and UV-light (Figure 5(B)). As shown in Figure 5(B), the DOX encapsulated nanocarrier at concentrations of approximately 100 $\mu\text{g mL}^{-1}$ showed enhanced cytotoxicity (~87 %) compared

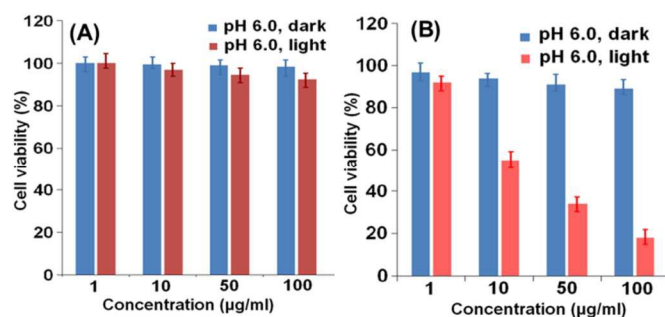


Figure 5. Cell viability of MCF-7 cells with various concentrations of blank and DOX loaded MSH@Azo-CA nanospheres in the absence and presence of UV-light (365 nm) at pH 6.0. (A) Blank samples at pH 6.0, dark and pH 6.0, UV-light. (B) DOX loaded samples at pH 6.0, dark and pH 6.0, UV-light.

to the nanocarrier concentrations of 1, 10 and 50 $\mu\text{g mL}^{-1}$. This suggests that the cytotoxicity of the nanocarriers is concentration dependent, which is responsible for the increased amount of drugs into the cells. The MTT assay confirmed the effects of the combined stimuli (external UV-light and intracellular pH), indicating that the designed MSH@Azo-CA nanospheres is desirable for tumor therapy.

Confocal laser scanning microscopic (CLSM) study

To examine the intracellular internalization of the Rh123-loaded MSH@Azo-CA particles, two sets of experiments were performed under different conditions, such as (A) dark, pH 6.0

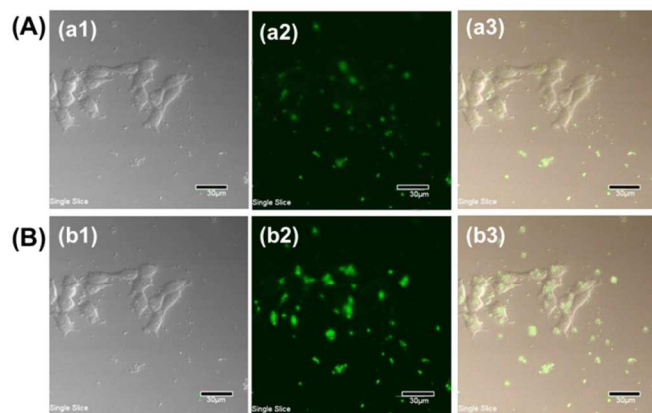


Figure 6. Confocal laser scanning microscopy images of the MCF-7 cells of Rh123 loaded MSH@Azo-CA nanospheres in the absence and presence of UV-light (365 nm). Rh123 loaded (A) pH 6.0, dark (a1-a3) and (B) pH 6.0, UV-light (b1-b3). Scale bar = 30 μm .

and (B) UV-light (365nm), pH 6.0, respectively. CLSM was used to observe the cellular internalization of the MSH@Azo-CA nanospheres as well as the combined stimuli-responsive efficient release of the encapsulated cargo molecules into the cells. To monitor this, Rh123 loaded MSH@Azo-CA particles were treated with MCF-7 cells under the following conditions: (i) dark, pH 6.0 (Figure 6A(a1-a3)); and (ii) UV-light, pH 6.0 (Figure 6B(b1-b3)) conditions. As shown in Figure 6((a2,a3) and (b2,b3) the green fluorescence suggests that the Rh123-loaded MSH@Azo-CA particles had been internalized by MCF-7 cells via an endocytosis process. Figure 6(A) shows that the green fluorescence intensity was not enhanced considerably under pH 6.0 and dark conditions. This indicates the strong binding of the cargo molecules with the guest binding $-\text{COOH}$, $-\text{NH}_2$ and $-\text{CONH}-$ sites as well as the efficient mesopore blockage by the 'trans-conformation' of the chrysoidine derivatives, which can act as efficient nanocontroller. Figure 6B shows considerably enhanced green fluorescence intensity and fluorescence area under acidic pH (pH 6.0) in the presence of UV-light (365 nm). This highlights the effects of the combined stimuli, i.e. the intracellular pH- and external UV-light triggered release of the loaded cargo from the MSH@Azo-CA carriers. The confocal microscopy results were in good agreement with the results obtained by the 'in vitro' release study (see Figure 4). Therefore, the results show that the synthesized MSH@Azo-CA nanospheres are quite

advantageous with the dual stimuli responsive-based, controlled/sustained release of a range of toxic anticancer drugs to the cancer cells in cancer therapy.

The UV-light driven dynamic motion of the diazo derivatives could be applicable to the controlled release of toxic cancer drugs with a predetermined dosage controlled by an 'ON' and 'OFF' trigger. Therefore, the MSH@Azo-CA system could be applicable to starting and stopping the release of the drugs by an external command. To validate this hypothesis, the Rh123 release from the Rh123-loaded MSH@Azo-CA nanospheres was also examined in an acidic pH medium (pH 5.0) with periodically turned 'ON' and 'OFF' states of UV-light exposure

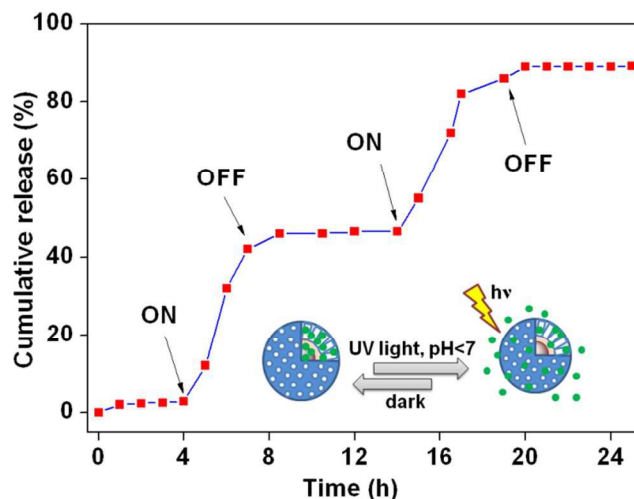


Figure 7. Partial release profile of Rh123 from the Rh123-loaded MSH@Azo-CA nanospheres as a function of the "ON-OFF-ON" UV-light trigger in an acidic pH (pH 5.0) release medium.

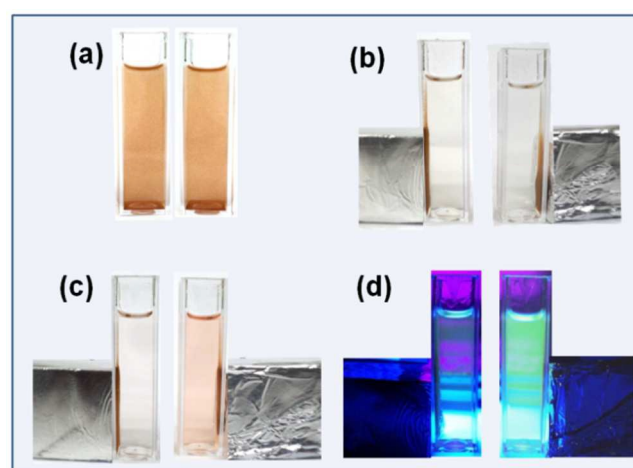


Figure 8. Rh123-loaded MSH@Azo-CA nanospheres were placed in two cuvettes dispersed in an aqueous solution at pH 5. Photographs were taken (a) without and (b) with external magnetic field. In the presence of an external magnetic field, the right cuvette was activated by UV-light (365 nm), and photographs were taken (c) before (left side cuvette) and after 4 h UV-light activation (right side cuvette) under (c) visible light and (d) UV irradiation.

(365 nm) at predetermined times (Figure 7). Figure 7 shows that the MSH@Azo-CA nanospheres can efficiently protect the payloads adequately under dark conditions, which allow them to diffuse from the carriers only upon exposure to UV-light, suggesting the possibilities of remote controlled drug release by an external 'ON' and 'OFF' command in acidic intracellular medium. Owing to the presence of a magnetic core, MSH@Azo-CA nanocarrier system can be utilized for magnetically-directed target drug delivery. To prove this hypothesis, 100 mg of Rh123-loaded MSH@Azo-CA particles were dispersed into two cuvettes in a PBS buffer solution at pH 5 (Figure 8). Both cuvettes were placed near a magnetic bar. As shown in Figure 8(a),(b), the nanocarrier particles were attracted to the walls of the cuvettes closest to the magnets. Subsequently, one cuvette (right hand side) was exposed to UV-light (365 nm) to promote the release of loaded Rh123, whereas the other cuvette (left hand side) was maintained under the dark conditions and treated as a reference. As shown in Figure 8(c,d), after 12 h exposure, the release medium of the right side cuvette changed to a pale pink and showed green fluorescence under UV-light (Figure 8(c)). In contrast, no considerable visible color and fluorescence of the release medium was observed in the reference cuvette (Figure 8(d)). Figure S5 shows photographs (inset) of the enhanced green fluorescence along with the UV-vis absorption curves of the Rh123 released in the release medium with respect to time in the presence of UV-light at pH 5. Overall, the MSH@Azo-CA nanospheres could be used for the loading and targeted delivery of anticancer agents to specific cancer sites directed by an external magnetic field and triggered by UV-light because the extracellular pH of the cancer tissues is more acidic ($< \text{pH } 7$)⁴² than the physiological pH, which can facilitate the release of loaded cargo molecules from the mesochannels of the MSH@Azo-CA nanospheres.

Conclusion

Novel core-shell magnetic mesoporous silica nanospheres with combined external (UV-light) and internal (intracellular pH) stimuli-responsive functional derivatives in the MSH@Azo-CA drug delivery system were synthesized. The UV-light sensitivity of the diazo part of the chrysoidine derivatives play an important role as nanogate and the surface $-\text{COOH}$, $-\text{NH}_2$ and $-\text{NH}-$ groups act as the drug binding sites through H-bonding/electrostatic interactions. The drug release characteristics of the MSH@Azo-CA nanospheres based on the external UV-light and pH of the release medium were investigated. The encapsulated payloads were released more efficiently in acidic environments (pH 6 and 5) under UV-light conditions than that in a physiological pH environment (pH 7.4) under dark conditions. The Rh123 release results showed that a combination of pH and UV-light stimuli-responsive properties would be desirable for drug delivery to the tumor sites in a controlled manner. The excellent combined UV-light and pH responsive release study of Rh123 from the MSH@Azo-CA system is expected to be valuable for the loading and delivery of various toxic anticancer agents in cancer therapy.

The MTT assay was performed using the anticancer drug (DOX)-loaded MSH@Azo-CA using MCF-7 cells to determine if the system could be applicable to the safe delivery of anticancer drugs. In addition, the cellular uptake properties were observed by confocal laser scanning microscopy. The efficient delivery of anticancer agents was observed in a controlled manner to the cancer sites by the 'ON' and 'OFF' command driven by external UV-light. In addition, the experimental results highlighted the feasibility of the target delivery of anticancer drugs to the cancer sites using an external magnetic field. Therefore, the designed MSH@Azo-CA carrier system could have potential applications in the target delivery of anticancer agents with a predetermined dose to specific cancer sites without being harmful to the normal tissues.

Acknowledgements

This work was financially supported by the '2015 Post-Doc. Development Program' of Pusan National University, Korea and the National Research Foundation of Korea (NRF) Grant funded by the Ministry of Science, ICT & Future Planning, Korea (Acceleration Research Program (NRF-2014R1A2A1A11054584) and Brain Korea 21 Plus Program (21A201380002)).

^a Department of Polymer Science and Engineering, Pusan National University, Busan 46241, Korea.
E-mail: csha@pnu.edu

^b Department of Biochemistry, School of Medicine, Pusan National University, Yangsan Hospital, Yangsan 50612, Korea

† Electronic supplementary information (ESI) available: SEM, TEM, particle size distribution, TGA, magnetization curves.

References

- 1 C. J. Ke, T. Y. Su, H. L. Chen, H. L. Liu, W. L. Chiang, P. C. Chu, Y. N. Xia, H. W. Sung, *Angew. Chem. Int. Ed.* 2011, **50**, 8086.
- 2 R. Cheng, F. H. Meng, S. B. Ma, H. F. Xu, H. Y. Liu, X. B. Jing, Z. Y. Zhong, *J. Mater. Chem.* 2011, **21**, 19013.
- 3 A. K. Varkouhi, M. Scholte, G. Storm, H. J. Haisma, *J. Control. Release*, 2011, **151**, 220.
- 4 T. M. Allenand, P. R. Cullis, *Science*, 2004, **303**, 1818.
- 5 S. Chandra, S. Mehta, S. Nigam, D. Bahadur, *New. J. Chem.* 2010, **34**, 648.
- 6 W. Al-Jamal, K. Kostarelos, *Acc. Chem. Res.* 2011, **44**, 1094
- 7 K. S. Soppimath, T. M. Aminabhavi, A. R. Kulkarni, W. E. Rudzinski, *J. Control. Release*, 2001, **70**, 1
- 8 J. Yang, D. Shen, L. Zhou, W. Li, X. Li, C. Yao, R. Wang, A. Mohamed El Toni, F. Zhang, D. Zhao, *Chem. Mater.* 2013, **25**, 3030
- 9 M. Arruebo, R. Fernandez-pachaco, S. Inesta, J. Arbiol, M. Ibarra, J. Santamaria, *Nanotechnology*, 2006, **17**, 4057.
- 10 J. Lu, E. Choi, F. Tamanoi, J. I. Zink, *Small*, 2008, **4**, 421.
- 11 X. Guoand, F. C. Jr Szoka, *Acc. Chem. Res.* 2003, **36**, 335.
- 12 I. I. Slowing, B. G. Trewyn, V. S. Lin, *J. Am. Chem. Soc.* 2006, **128**, 14792.

- 13 T. Xia, M. Kovoichich, M. Liong, H. Meng, S. Kabehie, S. Geopge, J. I. Zink, A. E. Nel, *ACS Nano*, 2009, **3**, 3273.
- 14 I. I. Slowing, J. I. Vivero-Escoto, C. -W. Wu, V. S. Y. Lin, *Adv. Drug. Deliv. Res.* 2008, **60**, 1278.
- 15 J. Kim, J. E. Lee, J. Lee, J. H. Yu, B. C. Kim, K. An, Y. Hwang, C. -H. Shin, J. G. Park, J. Kim, T. Hyeon, *J. Am. Chem. Soc.* 2006, **128**, 688.
- 16 M. Liong, J. Lu, M. Kovoichich, T. Xia, S.G. Ruehm, A.E. Nel, F. Tamanoi, J. I. Zink, *ACS Nano*, 2008, **2**, 889.
- 17 H. Amiri, K. Saeidi, P. Borhani, A. Manafirad, M. Ghavami, V. Zerbi, *ACS Chem. Neurosci.* 2013, **4**, 1417.
- 18 J. E. Lee, N. Lee, H. Kim, J. Kim, S. H. Choi, J. H. Kim, T. Kim, I. C. Song, S. P. Park, W. K. Moon, T. Hyeon, *J. Am. Chem. Soc.* 2010, **132**, 552.
- 19 L. Zhang, T. Wang, L. Yang, C. Liu, Y. A. Wang, Z. Su, *Chem. Eur. J.* 2012, **18**, 12512.
- 20 J. Fan, C. Yu, F. Gao, J. Lei, B. Tain, L. Wang, Q. Luo, B. Tu, W. Zhou, D. Zhao, *Angew. Chem. Int. Ed.* 2003, **42**, 3146.
- 21 A. Popat, J. Lie, G. Q. Lu, S. Z. Qiao, *J. Mater. Chem.* 2012, **22**, 11173.
- 22 L. Tan, H.-X. Wu, M.-Y. Yang, C.-J. Liu and R.-X. Zhuo, *RSC Adv.* 2015, **5**, 10393.
- 23 L. Tan, M.-Y. Yang, H.-X. Wu, Z.-W. Tang, J.-Y. Xiao, C.-J. Liu and R.-X. Zhuo, *ACS Appl. Mater. Interfaces*, 2015, **7**, 6310.
- 24 C. Y. Lai, B. G. Trewyn, D. M. Jeftinija, K. Jeftinija, S. Xu, S. Jeftinija, V. S. Y. Lin, *J. Am. Chem. Soc.* 2003, **125**, 4451.
- 25 K. C. F. Leung, T. D. Nguyen, J. F. Stoddart, J. I. Zink, *Chem. Mater.* 2006, **18**, 5919.
- 26 Y. Zhu, M. Fujiwara, *Angew. Chem. Int. Ed.* 2007, **119**, 2291.
- 27 P. Yang, S. Gai, J. Lin, *J. Chem. Soc. Rev.* 2012, **41**, 3679.
- 28 C. Alvarez-Lorenzo, L. Bromberg, A. Conchiro, *Photochem. Photobiol.* 2009, **85**, 848.
- 29 J. Yang, D. Shen, L. Zhou, W. Li, X. Li, C. Yao, R. Wang, A. M. El-Toni, F. Zhang, D. Zhao, *Chem. Mater.* 2013, **25**, 3030.
- 30 Y. Zhao, L. -N. Lin, Y. Lu, H.-L. Gao, S. F. Chen, P. Yang, S. -H. Yu, *Adv. Healthcare Mater.* 2012, **1**, 327.
- 31 S. Wu, X. Huang and X. Du, *Angew. Chem. Intl. Ed.* 2013, **52**, 5580.
- 32 X. Huang, N.P. Young and H.E. Townley, *Nanomater Nanotechnol.* 2014, **4**, doi: 105772/58290.
- 33 C. Chen, F. Pu, Z. Huang, Z. Li, J. Ren and X. Qu, *Nucleic Acids Res.* 2011, **39**, 1638.
- 34 A. V. Jovanoic, J. A. Flint, M. Varshiney, T. E. Morey, D. M. Dennis, R. S. Duran, *Bio Macromol.* 2006, **7**, 945.
- 35 P. Yang, Z. W. Quan, Z. Y. Hou, C. X. Li, X. J. Kang, Z. Y. Cheng, J. Lin, *Biomaterials*, 2009, **30**, 4786.
- 36 Z. Teng, X. Zhu, G. Zheng, F. Zhang, Y. Deng, L. Xiu, W. Li, Q. Yang, D. Zhao, *J. Mater. Chem.* 2012, **22**, 17677.
- 37 D. L. Harp, *Anal. Chim. Acta*, 1997, **346**, 373.
- 38 F. Y. Cheng, C. H. Su, Y. S. Yang, C. S. Yeh, C. Y. Tsai, C. L. Wu, M. T. Wu, D. Shieh, *Biomaterials*, 2005, **26**, 729.
- 39 M.S. Moorthy, D.-J. Seo, H.-J. Song, S. S. Park, C.-S. Ha, *J. Mater. Chem. A*, 2013, **1**, 12485.
- 40 C. P. Beam, *J. Appl. Phys.* 1959, **30**, 120.
- 41 T. Tanaka, H. Ogino, M. Iwamoto, *Langmuir*, 2007, **27**, 11417.
- 42 U. Shamim, S. Hanif, A. Albaniyan, F. W. J. Beck, B. Bao, Z. Wang, S. Banerjee, F. H. R. M. Sarkar, S. M. Mohammad Hadi, A. Hasmi, *J. Cell Physiol.* 2012, **227**, 1493.

Table of Contents

Design of core-shell magnetic mesoporous silica hybrids for pH and UV-light stimuli-responsive cargo release

Madhappan Santha Moorthy,^a Hak-Bong Kim,^b Jae-Ho Bae,^b Sun-Hee Kim,^b and Chang-Sik Ha^{*a}

A controlled drug release system has been proposed. The drug carrier system efficiently works under combined (i) UV-light and (ii) pH triggers for controlled release of model cargoes. The cytotoxicity of the core-shell hybrid were examined using MCF-7 cells. The designed nanocarrier system also have potential use in the targeted delivery of cargoes by the 'ON' and 'OFF' command by the external UV-light trigger.

